JOURNAL OF SYNCHROTRON RADIATION
ISSN 1600-5775

Direct non-destructive total reflection X-ray fluorescence elemental determinations in zirconium alloy samples

Kaushik Sanyal,[a]* Buddhadev Kanrar,[a,b] Sangita Dhara,[a,b] Mirta Sibilia,[c] Arijit Sengupta,[d,b] Andreas Germanos Karydas[e] and Nand Lal Mishra[a,b]‡

[a]Fuel Chemistry Division, Bhabha Atomic Research Centre, Trombay, Mumbai 400085, India, [b]Homi Bhabha National Institute, Anushaktinagar, Mumbai 4000 094, India, [c]IAEA-XRF Beamline, Elettra Sinchotrone Trieste, Trieste, Italy, [d]Radiochemistry Division, Bhabha Atomic Research Centre, Mumbai 400 085, India, and [e]Institute of Nuclear and Particle Physics, NCSR 'Demokritos', Agia Paraskevi 153 10, Greece.
*Correspondence e-mail: kaushik.sanyal88@gmail.com, ksanyal@barc.gov.in

Received 15 May 2020
Accepted 9 July 2020

Edited by P. A. Pianetta, SLAC National Accelerator Laboratory, USA

‡ Retired (current email: nlmisra@yahoo.com).

Keywords: Zircalloy; non-destructive analysis; TXRF; synchrotron; low- and high-Z elements.

Supporting information: this article has supporting information at journals.iucr.org/s

The development of a direct non-destructive synchrotron-radiation-based total reflection X-ray fluorescence (TXRF) analytical methodology for elemental determinations in zirconium alloy samples is reported for the first time. Discs, of diameter 30 mm and about 1.6 mm thickness, of the zirconium alloys Zr-2.5%Nb and Zircalloy-4 were cut from plates of these alloys and mirror polished. These specimens were presented for TXRF measurements directly after polishing and cleaning. The TXRF measurements were made at the XRF beamline at Elettra synchrotron light source, Trieste, Italy, at two different excitation energies, 1.9 keV and 14 keV, for the determinations of low- and high-*Z* elements, respectively. The developed analytical methodology involves two complementary quantification schemes, *i.e.* using either the fundamental parameter method or relative sensitivity based method, allowing quantification of fifteen minor and trace elements with respect to Zr with very good precision and accuracy. In order to countercheck the TXRF analytical results, some samples were analyzed using the DC arc carrier distillation atomic emission spectrometry technique also, which shows an excellent agreement with the results of the TXRF-based methodology developed in this work. The present work resulted in a non-destructive TXRF elemental characterization methodology of metal and alloy samples avoiding the cumbersome dissolution and matrix separation which are normally required in other techniques and traditional methods of TXRF determination. In addition, the production of analytical waste could also be avoided to a large extent. Although the work was carried out for specific applications in the nuclear industry, it is equally suitable for other such samples in different industrial applications.

1. Introduction

Zirconium and its alloys find great importance and application in the nuclear industry. Different alloys of zirconium are used as cladding materials, pressure tubes, *etc*. in different types of reactors. Zr–Nb alloys are generally used as pressure tubes in pressurized heavy water reactors, where Nb is added to increase the mechanical strength of the material (Choudhuri *et al.*, 2008). Zircalloy is used as cladding material in pressurized water reactors as well as boiling water reactors (Arsene *et al.*, 2003). The chemical, mechanical and thermo-physical properties as well as the neutron economy are very much dependent on the composition of these alloys (Northwood, 1985). There are stringent specification limits of the amount of different trace elements present in these alloys which have to be strictly monitored and maintained during their fabrication

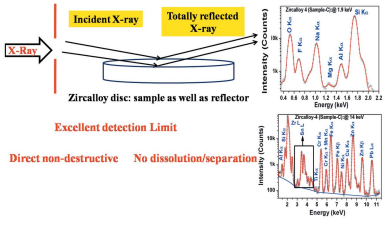

for the safe and efficient operation of the reactors. These specifications are set by the reactor physicists on the basis of the type of reactor (Paul *et al.*, 2010; Zaimovskii, 1978).

Several analytical techniques, *e.g.* inductively coupled plasma mass spectrometry, atomic emission spectrometry, atomic absorption spectrometry, electrothermal atomic absorption spectrometry, spark source mass spectrometry, glow discharge mass spectrometry, chromatography, *etc*., are available for trace elemental analysis in zirconium matrices (Steffan & Vujicic, 1994; Shenkey & Fuchung, 1990; Robinson & Hall, 1987; Manjusha *et al.*, 2013). Most of these techniques require dissolution of the alloy followed by separation of the major matrix zirconium. The dissolution of zirconium itself is a highly tedious as well as time-consuming job requiring handling of concentrated corrosive acids and heating (Vander Wall & Whitener, 1959). In addition, it is very difficult to separate the matrix selectively from some analytes. For example, Hf, having very high neutron absorption cross section, is an undesirable element in nuclear fuel and structural materials. It is very difficult to separate Hf from Zr by the solvent extraction method (Banda *et al.*, 2012). Moreover, during dissolution and matrix separation procedures, there is a probability that additional impurities may be introduced in the sample solutions. Therefore, non-destructive analytical methods are always desirable for elemental characterization of such samples, as such methods require minimum sample preparation and avoid the dissolution as well as separation steps (Acharya *et al.*, 2004; Dhara *et al.*, 2015). For radioactive materials, the non-destructive methods have an added advantage of producing no or a very small amount of analytical waste. Some analytical techniques requiring minimum sample preparation available for elemental analysis of different samples are instrumental neutron activation analysis, DC arc carrier distillation and laser-induced breakdown spectroscopy (Al-Jobori, 1988; Iofrida *et al.*, 2015; Pathak *et al.*, 2014). However, these techniques have their own limitations; for example, in instrumental neutron activation analysis, the sample has to be irradiated for a long time inside a nuclear reactor which is not easily available for routine analytical work. With the DC arc carrier distillation technique, refractory materials are difficult to analyze, whereas laser-induced breakdown spectroscopy is a technique that always requires standards of similar matrix composition.

X-ray fluorescence (XRF) is a very useful non-destructive elemental analysis technique for the analysis of different types of samples. Synchrotron-radiation-induced microprobe XRF analysis coupled with Monte Carlo simulation has already been reported for the determination of trace impurities in Zircalloy samples (Yilmazbayhan *et al.*, 2003). However, the attainable limits of detection in XRF, even at synchrotron facilities, during normal measurements (without using specialized instruments and highly optimized experimental conditions), are not adequate for checking compliance with the required specifications, *e.g.* the specifications for Cu and Ni are 50 and 70 p.p.m., respectively, in Zircalloy-4 (Weidinger, 2007). In addition, XRF analysis has severe matrix effects, and matrix matched calibration standards are recommended for accurate quantitative analysis (Bertin, 2012). Total reflection X-ray fluorescence (TXRF) analysis is a variant of XRF (Misra, 2011; Sanyal & Misra, 2019; Sanyal, Chappa *et al.*, 2018; Sanyal, Dhara & Misra, 2018). Under the TXRF excitation geometry, the exciting X-ray beam is made to fall on the surface of a polished substrate (reflector) at an incident angle much smaller than the so-called critical angle, ϑ_{crit}, for external total reflection resulting in very shallow penetration of the X-ray beam to the extent of only a few nanometres depth within the substrate (Klockenkämper & Bohlen, 2015; Wobrauschek, 2007; Kregsamer, 1991). On the other hand, trace elements within the sample dried residues on the top of the reflector or even impurities of the reflector materials are optimally excited with a significantly improved signal-to-noise ratio compared with that achieved in conventional XRF analysis. It is important to note that, when the purity of a semiconductor material (Si or Ge wafer) is studied, angular-resolved measurements at grazing incidence [grazing-incidence XRF (GIXRF)], in a typical range of zero up to 1–2° ($\gg \vartheta_{crit}$), can provide a distinct intensity profile of the analyte characteristic X-rays and clear differentiation between surface contamination and matrix impurities or dopants (Klockenkämper & Bohlen, 2015; Pianetta *et al.*, 2000; Pahlke *et al.*, 2001; Leenaers & Boer, 1995; De Boer *et al.*, 1991; Ingerle, Meirer *et al.*, 2014). In the conventional TXRF analysis, a few microlitres of the sample solution are deposited onto a clean quartz sample support along with an internal standard to form a very thin film that poses negligible matrix effect. Although TXRF analysis requires a very small amount of sample, solid samples are required to be dissolved and the major matrix has to be separated to obtain a thin film of the sample, free from matrix effects, deposited on the TXRF support (Sanyal, Dhara & Misra, 2018). Due to the above-mentioned features, TXRF has comparable (even improved in some cases) detection limits with the well established trace element analysis techniques. The quantification in TXRF analysis is commonly achieved by spiking the sample with a known concentration of a reference element (internal standard). A standard-free quantitative XRF analysis approach that actually utilizes the substrate fluorescence intensity calculated and measured at few incident angles has been recently proposed for calibration and quantification (Szaloki *et al.*, 1999). The quantification algorithm is based on the so-called fundamental parameter approach accounting properly for excitation conditions, physical interactions within the sample/substrate system and the irradiation and detection geometry.

The difficulty in the effective dissolution of zirconium-based alloys appears to be the major problem for its TXRF analysis. If a non-destructive TXRF-based analytical methodology can be developed for these alloys, it can substantially simplify the quality control of Zr-based reactor materials. Such an approach has been used for the ultra-trace non-destructive determination of trace contaminants in Si-wafer samples and TV glass samples (Pianetta *et al.*, 2000; Pahlke *et al.*, 2001; Ingerle, Schiebl *et al.*, 2014; Leenaers & De Boer, 1995). This novel approach may be feasible for the TXRF elemental determinations in zirconium-based alloys if the samples are

properly cut in the form of circular sample discs compatible with the TXRF spectrometer sample chamber and are mirror polished for direct TXRF measurements. The incident X-ray beam must impinge on these supports below the critical angle corresponding to the sample matrix. By satisfying the TXRF conditions, almost all the elements present on the surface of a sample can be excited very efficiently with minimum background. Under these excitation conditions, the matrix effects can be ignored due to the very limited penetration depth of the exciting beam (a few nanometres only) and the elemental quantification can be performed by means of predetermined relative sensitivity values obtained from the conventional TXRF measurements of standard solutions. In the proposed methodology, there is no requirement of matrix matching calibration standards, whereas the contained trace elements can be quantified versus the matrix dominant elements (Zr or Zr + Nb in the present case).

In this work, we have developed a non-destructive TXRF-based analytical method for trace elemental determinations in zirconium-based alloys using synchrotron radiation as an excitation source. The developed TXRF-based method is free from matrix effects. Low-*Z* elements like Na, Mg, Al, *etc*. could be probed optimally using a low-energy exciting beam (1.9 keV) whereas other elements could be determined using a higher-energy beam (14 keV) obtained due to the energy tunability of synchrotron radiation. Overall, the developed methodology is very simple, straightforward, less time consuming, avoids cumbersome sample dissolution and matrix separation and can be applied very efficiently for trace element determinations in different types of alloy materials. These features make this methodology very important for quality control purposes of metals and alloys. In addition, the production of analytical waste is negligible. The application of the proposed TXRF analytical methodology with these novel features for trace element determinations in Zr-based alloys is described in this paper.

2. Experimental

2.1. Sample preparation

Merck ICP single-element standard solutions of Na, Mg, Al, K, Ti, Cr, Mn, Co, Ni, Ga and Se having elemental concentration of 1000 μg ml^{-1} were mixed together and diluted to obtain 25 μg ml^{-1} elemental concentrations of each element in the resultant solution STD-1. This solution was used for determining relative sensitivity values of respective *Kα* X-ray emission lines with respect to Ga *Kα*. Similarly, another standard solution STD-2 was prepared by mixing Merck ICP single-element standard solutions of Ga, Zr, Nb, Mo, Sn, Ba, and W having elemental concentration of 1000 μg ml^{-1} to obtain resultant concentrations of each element of 25 μg ml^{-1}. This solution was used for measurement of the relative sensitivities of the *Lα* X-ray lines with respect to Ga *Kα*. In both these standard solutions, Ga was used as an internal standard. Suprapure concentrated HNO_3 diluted to 5% with Milli-Q water, having a specific resistance of 18.2 MΩ, was used to dilute the samples and standards. Aliquots of 5 μL of each standard solution mixture were deposited on clean flat polished quartz sample supports in triplicate by drying in ambient atmosphere to form thin films of samples on the sample supports.

Two Zr-2.5%Nb alloy (Sample-A and Sample-B) and two Zircalloy-4 (Sample-C and Sample-D) circular discs of 30 mm diameter and about 1.6 mm thickness were cut from respective sheets. These discs were mirror polished using diamond paste. The diamond paste was spread on a polishing cloth which was attached with a polishing machine for polishing the samples. The diamond pastes are available in different coarse grades, and one having a coarse size of 6–14 μm was used for lapping and pre-polishing. Later another paste having a coarse size of 0.3–3 μm was used for final polishing to obtain mirror finished surfaces. The roughness of the thus prepared discs was checked with an optical profilometer and estimated to be around 50 nm which is well below the critical roughness required (100 nm) to achieve TXRF conditions (Klockenkämper & Bohlen, 2015). The polished discs were first cleaned with ultrapure ethanol and later wiped with clean tissue paper. Finally, the discs were washed with Milli-Q water to remove any surface impurities present on them, dried and used for TXRF measurements directly. The surface flatness of the thus prepared discs was further ensured by physical observation of the total reflection of X-rays falling at these surfaces below critical angles. In such a situation the direct as well as totally reflected beams were observed separately one above the other when the angle of incidence of the X-ray beam was adjusted to 70% of the critical angle. This observation indicates that the surfaces are quite flat and fit for TXRF measurements. The absence of surface impurities on the discs was further confirmed by the GIXRF measurements.

2.2. TXRF measurements

The TXRF measurements were carried out at the XRF beamline of the Elettra synchrotron, Trieste, Italy. The beamline currently delivers exciting X-ray beams in different energy regions with the help of a Si (111) double-crystal monochromator (2–20 keV) and three multi-layers (low energy: 700–1800 eV; medium energy: 1500–8000 eV; high energy: 3600–14000 eV). The TXRF measurements were carried out at 14 keV (RuB_4C multilayer) with a 130 μm-thick carbon filter (transmission 1.7% @ 2.3 keV) to minimize the contribution of low-energy harmonics and at 1.9 keV (Ni-C multilayer) without the use of any filter. The beam size at the sample position was 200 μm (H) × 100 μm (V). The sample holder can accommodate four samples having 30 mm diameter and 1–3 mm thickness at each loading. Fig. 1 shows an image of the sample holder containing four samples (two Zr-2.5%Nb and two Zircalloy-4 samples) having 30 mm diameter and 1.6 mm thickness. The samples are first introduced into the load lock chamber. After attaining a certain vacuum level ($<10^{-6}$ mbar), the samples are finally transferred into the main sample chamber: an ultrahigh-vacuum (UHV) chamber (IAEAXspe instrument) maintained at 10^{-8} mbar pressure.

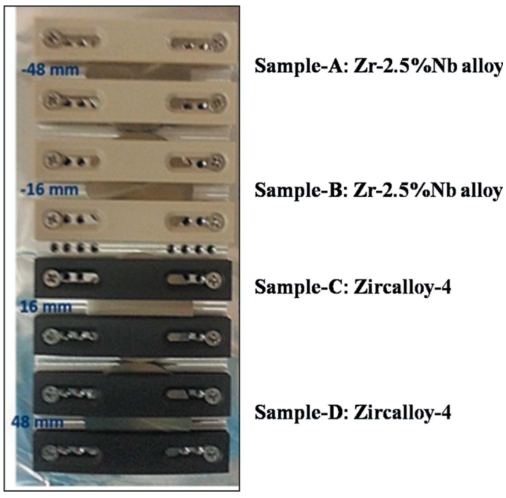

Figure 1
Photograph of samples loaded in sample containment arrangement inside the ultrahigh-vacuum chamber for TXRF measurements at the XRF beamline, Elettra Sincrotrone Trieste, Italy.

The sample holder is attached to a five-axis motorized sample manipulator which consists of an *XYZ* linear translation stage, high-precession θ and φ goniometer. A silicon drift detector (Bruker Nano GmbH, X-Flash 5030) having 30 mm^2 nominal area, 450 µm crystal thickness and an energy resolution of 131 eV (full width at half-maximum) at 5.9 keV (Mn $K\alpha$) was used for detection and measurement of X-rays. The detector is equipped with a Super Light Element Window (SLEW) of the type AP3 (polymer) having an estimated thickness of ∼363 nm, covered by ∼70 nm of Al and supported by a silicon grid having 77% open area. The detector-to-sample distance was 11 mm. More details about the beamline and IAEAXspe instrumentation and operation are described in detail elsewhere (Karydas *et al.*, 2018; Sanyal, Kanrar *et al.*, 2017).

It is very much necessary to maintain the TXRF conditions during the measurements so that the background counts are minimum, and the undesired matrix effects are negligible during the TXRF analysis. The Zircalloy samples were mirror polished to obtain a very smooth surface suitable for the total reflection of X-rays. For TXRF measurements a grazing angle equal to about 70% of the critical angle was set by performing vertical *X* scans with a step size of 0.1 mm (Klockenkämper & Bohlen, 2015). For fulfilling the TXRF conditions for a particular substrate material there are several steps involved in the alignment procedure which are described in detail in the literature (Sanyal, Kanrar *et al.*, 2017).

During GIXRF measurements of the Zr-2.5%Nb sample, 14 keV excitation energy was used and angular scans were performed from 0 to 4.5°, divided into two parts: the first part, 0–2°, was scanned at angular steps of 0.005° and the second part, in the range 2–4.5°, was scanned with angular steps of 0.01°. Each angular scan was measured for a live time of 15 s. The intensities of the detected characteristic X-rays were normalized with respect to the charge collected by the entrance diamond-based photodiode that serves as the beam monitoring system of the XRF beamline.

The obtained TXRF spectra were evaluated using the *PyMca* software package (Solé *et al.*, 2007). The spectral data fitting involves a least-squares fitting methodology by minimizing the χ^2 value. During the analysis of the TXRF spectra, two separate methods were used: the fundamental parameter (FP) method and the relative sensitivity based method. The FP approach is based on the theoretical relationship between the measured intensities of X-rays and elemental concentrations (Szalóki *et al.*, 2019). To achieve a reliable quantification, the experimental set-up and instrumental parameters, such as incident/outgoing angles, sample matrix composition, as well as the X-ray detector characteristics (type and thickness of the window material, thickness of the Si crystal *etc.*), were introduced within the *PyMca* software (Karydas *et al.*, 2018). It should be noted that at the TXRF excitation condition the incident beam probes a depth of only a few nanometres below the surface of the material being analyzed and described by the so-called minimum penetration depth which is insensitive to the energy of the impinging radiation and depends on the atomic weight, atomic number and density of the material (Klockenkämper & Bohlen, 2015; Szalóki *et al.*, 2019). The penetration depth was estimated to be ∼ 2 nm and this probed sample thickness was introduced into *PyMca* to account for the rather negligible sample self-absorption correction (Szaloki *et al.*, 1999). Finally, the FP-based concentrations of the contained minor and trace elements in the Zr-based alloys were deduced on a relative basis versus the dominant elements (Zr or Zr + Nb) concentration.

2.3. DC arc carrier distillation measurement

In order to validate the TXRF analytical results, two samples, Zr-2.5%Nb (Sample-A) and Zircalloy-4 (Sample-C), were analyzed using the DC arc carrier distillation method also. The samples were cut in the form of very small fine turnings. A Spectro-Arcos Model Arcos FHS12 ICP-AES with a high-performing capacitive coupled device (CCD) as the detector and DC arc as the excitation source was used for the DC arc analysis. The unit is equipped with linear arrays of CCD detectors arranged in a Paschen-Runge mount having a focal length of 750 mm, fitted with three holographic gratings, two of them with 3600 grooves mm^{-1} and one with 1800 grooves mm^{-1}. This arrangement enables wavelength coverage of 130–770 nm in the first order. The spectrometer provides a resolution of 0.01 nm in the 130–340 nm region and 0.02 nm in the wavelength region greater than 340 nm (Sengupta *et al.*, 2016). A solution of 5% AgCl was used as carrier to sweep out the analytes into the arc leaving Zr as refractory matrix oxide (Sengupta *et al.*, 2014). SpecPure grade oxides of individual elements (AgCl supplied by SPEX Industries, USA, and high-purity pre-analyzed ZrO_2 procured from NFC Hyderabad, India), which served as base materials, were used for preparation of the standards. Seven points standardization was carried out to establish calibration curves. Each sample was divided into three parts having almost similar weight (∼50 mg) and each specimen was measured

independently. The data reported here are within a 96% confidence limit, *i.e.* 2σ.

3. Results and discussions

The *PyMca*-fitted TXRF spectra of standard solutions obtained with an excitation energy of 14 keV are shown in Figs. 2(*a*) (STD-1) and 2(*b*) (STD-2). The respective TXRF spectrum for STD-1 using an excitation energy of 1.9 keV, mainly for low-*Z* excitation, is shown in Fig. 2(*c*) (*K* lines). All spectra present excellent peak statistics, even for the low-*Z* elements (F, Na, Mg, Al) excited by the 1.9 keV beam [Fig. 2(*c*)]. The presence of the F *Kα* peak in the spectra is seen because Na was taken as NaF for making the Na standard solution. To calculate the detection limits these spectra were also analyzed using the IAEA-QXAS (Quantitative X-ray Analysis System) package software named *AXIL* (*Analysis of X-ray spectra by Iterative least Squares*), as *PyMca* software does not give information about the background counts (Vekemans *et al.*, 1994). The background counts obtained from the IAEA-QXAS software were used for calculation of detection limits (DL) using the following formula,

$$\mathrm{DL} = \frac{3\sqrt{I_\mathrm{B}}}{I_\mathrm{P}}\, m_i, \qquad (1)$$

where I_B is the area under the background (obtained from processing of spectra by *AXIL*), I_P is the area of the peak of the analyte line of interest (obtained from processing spectra by *PyMca*) and m_i is the mass of the analyte (or it may be the concentration of the analytes to obtain detection limits in concentration units) on the TXRF support during measurements (Sanyal, Dhara & Misra, 2017). The detection limits obtained using different excitation energies are given in Table 1. It can be seen that the detection limits obtained using 1.9 and 14 keV excitation energies are sufficient for the non-destructive TXRF-based trace elemental analysis in alloy samples.

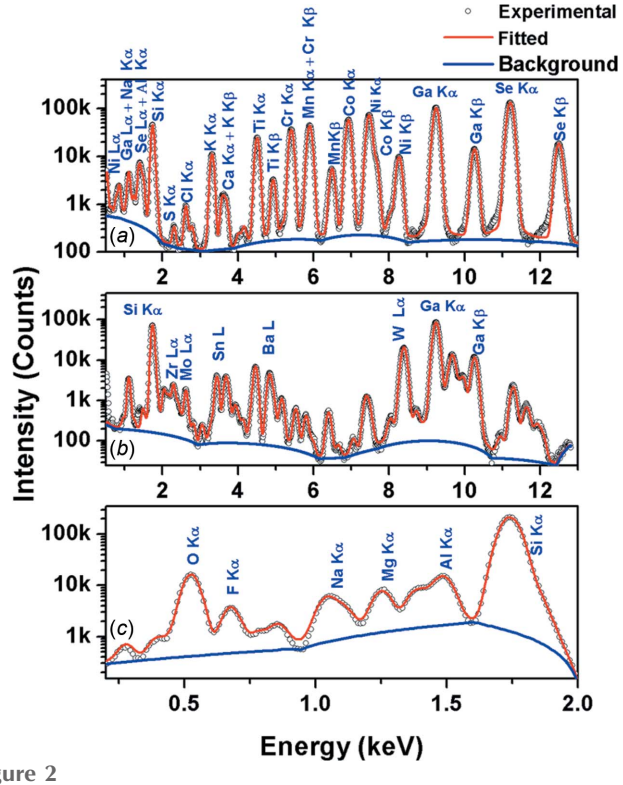

Figure 2
PyMca-fitted TXRF spectra. (*a*) STD-1 (*K* lines), (*b*) STD-2 (*L* lines), using 14 keV excitation energy; and (*c*) STD-1 (*K* lines, low-*Z* elements) using 1.9 keV excitation energy.

Table 1
Detection limits of different elements obtained from TXRF spectra measured with excitation energies of 1.9 keV and 14 keV and measurement time of 1000 s (live time).

Element	Excitation energy	Analytical line	Detection limit (ng mL^{-1})
F	1.9 keV	*Kα* lines	578
Na			304
Mg			209
Al			105
K	14 keV	*Kα* lines	26
Ti			12
Cr			8
Mn			8
Co			6
Ga			5
Se			4
Zr		*Lα* lines	360
Mo			48
Sn			23
Ba			13
W			4

The relative sensitivities of both *Kα* and *Lα* X-ray emission lines were calculated separately from the TXRF spectra of their respective standard solutions measured using 14 and 1.9 keV excitation energies. The relative sensitivities were calculated with respect to Ga *Kα* using Ga as an internal standard while exciting the samples with 14 keV energy. However, while using 1.9 keV excitation energy, relative sensitivities were determined with respect to Al *Kα* as Al *Kα* can be excited by both exciting energies (14 and 1.9 keV). Fig. S1 of the supporting information shows relative sensitivity plots of both *Kα* and *Lα* lines with respect to Ga *Kα*. The trend observed in both curves, namely a gradual increase of sensitivity values with respect to the atomic number of the analytes, indicates that the TXRF conditions are well satisfied in both cases (Klockenkämper & Bohlen, 2015). The plots were fitted using a polynomial function of order three with good correlation coefficient in both cases. It should also be mentioned that, since the maximum excitation energy available for measurements at the XRF beamline (14 keV) is not sufficient to excite the Zr *Kα* as the Zr *K* absorption edge energy (17.997 keV) is well above this energy (14 keV), the Zr *Lα* line was used as an analytical line for Zr. While using 14 keV excitation energy, the TXRF elemental concentrations in alloy samples were determined with respect to Zr (with Zr = 100% in Zircalloy and 97.5% in Zr-2.5% Nb alloys) using the respective sensitivity values determined, and the concentration of Al thus obtained was used as an internal standard for low-*Z* element determinations using 1.9 keV excitation. Later

the concentrations of all elements including Zr were normalized to a total of 100%.

The fitted TXRF spectra of Sample-A and Sample-C using 14 keV excitation energy are shown in Fig. 3. It can be observed that the *K* X-ray lines of different elements like Al, Si, Ca, Ti, Cr, Mn, Fe, Ni, Cu, Zn, *etc*. were detected with good statistics in both samples. Fig. 3 shows that the Zr and Nb *L* X-ray emission lines are almost merged with each other in the spectrum of Sample-A (marked together as a rectangular box). This is because the energy of the Zr *Lα* ($E_{\text{Zr-}L3M5}$ = 2.042 keV) and Nb *Lα* ($E_{\text{Nb-}L3M5}$ = 2.166 keV) emission lines are very closely spaced and cannot be resolved by the silicon drift detector. For this reason, the Nb concentrations are not reported in the present study and were assumed to be 2.5% in Zr-2.5% Nb alloys while calculating the elemental concentrations of the elements determined by TXRF in these alloys. This problem can be efficiently overcome by using an excitation energy above the *K*-shell threshold of Nb (18.98 keV), that could offer the possibility to detect and analyze properly both the Zr *Kα* and Nb *Kα* X-ray emission lines without any spectral interferences.

From Fig. 3, an appreciable intensity of the Pb *L* lines can be seen in both samples and the Sn *L* lines in the Zircalloy-4 sample. It can also be seen from Fig. 3 that the Hf *Lα* line (7.89 keV) is situated at the tail of the Cu *Kα* line (8.04 keV) in the case of the Zr-2.5%Nb alloy spectra. Being a neutron absorber Hf is a very important element in the chemical characterization of nuclear materials. There is spectral interference of Cu *Kα* with Hf *Lα* in the TXRF spectrum. However, this problem of interference was overcome by fitting the spectra by means of the *PyMca* software. Since the specifications for Hf in Zircalloy and Zr-2.5% Nb alloys are 200 and 50 p.p.m., respectively, it should be possible to determine such elements easily (Lenka, 2012). Fig. 4 shows the *PyMca*-fitted TXRF spectra of Zr-2.5%Nb and Zircalloy-4 samples excited using 1.9 keV energy. It can be seen that the Zr *L* lines are minimally visible in both spectra (the Zr L_3 absorption edge is 2.22 keV, higher than that of the 1.9 keV excitation energy), thus confirming the effective operation of the beamline high-order suppressor which results in a negligible contribution of the first harmonic ($\sim 3.2 \times 10^{-4}$) within the exciting beam.

The energy of the exciting beam (1.9 keV) was selected considering the following requirements: (i) optimally ionize the low-*Z* elements [exciting energy > Si-*K* absorption edge (1.84 keV)]; (ii) eliminate the production of the Zr *L* lines [exciting energy < Zr-L_3absorption edge (2.222 keV)]; and (iii) minimize the effect of the *LM* resonant raman scattering (RRS) of the exciting beam on Zr atoms (the exciting energy is 322 eV below the Zr L_3 absorption edge), thus eliminating any possible spectral interference of the LM-RRS band, mostly with the *K*-lines of Si and to a less extent with Al and Mg (Jaklevic *et al.*, 1988; Karydas & Paradellis, 1999; Leani *et al.*, 2019; Pianetta *et al.*, 2000).

From Fig. 4 it can be observed that the O, F, Na, Mg, Al, Si, K, *etc*. *Kα* emission lines are clearly visible in both the spectra. In this case the relative sensitivities of all the elements were determined with respect to the Al *Kα* line which can be excited by both 1.9 keV and 14 keV energy X-ray beams. The concentration of Al present in the samples was determined

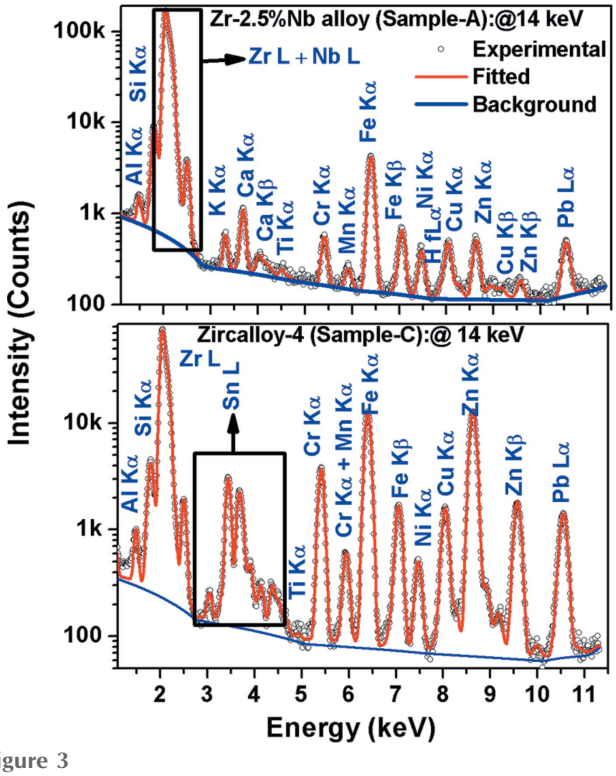

Figure 3
PyMca-fitted TXRF spectra of Zr-2.5% Nb (Sample-A) and Zircalloy-4 (Sample-C) samples using 14 keV excitation energy.

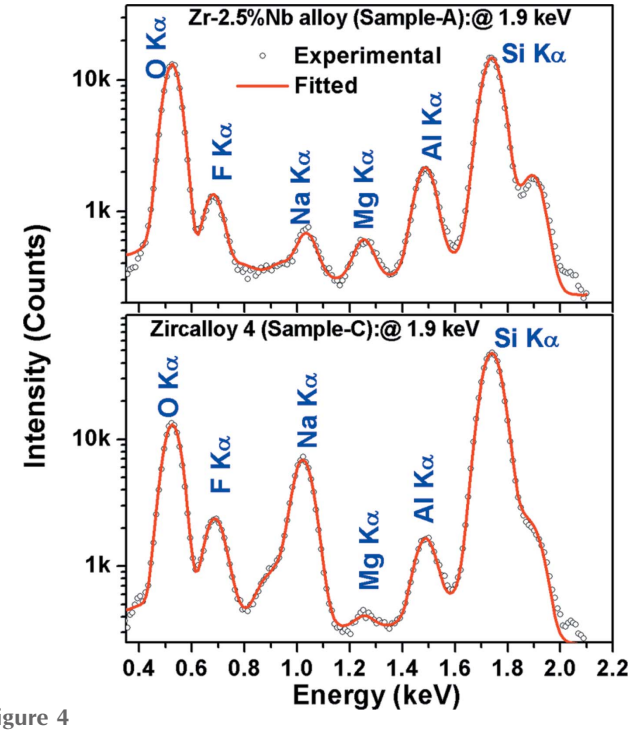

Figure 4
PyMca-fitted TXRF spectra of Zr-2.5%Nb (Sample-A) and Zircalloy-4 (Sample-C) samples excited using 1.9 keV excitation energy.

with respect to Zr using the high-energy beam (14 keV). This Al concentration was used as the concentration of the Al internal standard during the 1.9 keV excitation and the other low-Z elements excited using this low-energy beam (1.9 keV) were quantified using Al as an internal reference element. It should be noted, however, that for the quantitative analysis of Si it was finally decided to use the data resulting from the 14 keV excitation, as the effect of LM-RRS on Zr atoms has never been quantified as a function of the excitation energy. Fluorine is also a very important element in the quality assessment of Zr alloys because it is a very corrosive element. Clear peaks of F $K\alpha$ were visible in TXRF spectra of Zr alloys, but F was not quantified because unrealistic high fluorine concentrations were found. We could not find any possibility of or reason for surface contamination of samples by F. Probably, the spectral interference of F $K\alpha$ (0.677 keV) with the Fe $L\alpha$ (0.705 keV) and the presence of an elevated amount of Fe in the samples may be giving uncontrolled errors in the deconvolution of the F $K\alpha$ and Fe L profiles. This aspect requires further study.

Table 2
Comparison of TXRF-determined concentrations using the relative sensitivity values and FP approaches with the DC arc carrier distillation method for different trace elements in Sample A: Zr-2.5%Nb alloy.

The values in '±' indicate a standard deviation of 1σ for $n = 3$ for TXRF measurements and 2σ for $n = 3$ for DC arc measurements.

	Concentrations (μg g^{-1})				
Elements	RS value approach (normal) TXRF analysis (A)	Fundamental parameter approach TXRF analysis (B)	DC arc carrier distillation method (C)	A/B ratio	A/C ratio
Na	2700 ± 110	2400 ± 100	2300 ± 300	1.12 ±0.06	1.1 ± 0.1
Mg	810 ± 60	740 ± 50	800 ± 90	1.1 ± 0.1	1.0 ± 0.1
Al	4200 ± 70	3810 ± 60	4400 ± 700	1.10 ± 0.02	0.9 ± 0.1
Si	4700 ± 300	4700 ± 300	5000 ± 800	1.0 ± 0.1	0.9 ± 0.1
Ti	26 ± 1	24 ± 1	22 ±1	1.08 ± 0.06	1.18 ± 0.07
Cr	145 ± 3	129 ± 3	150 ± 3	1.12 ± 0.03	0.96 ± 0.02
Mn	21 ± 1	18 ± 1	19 ± 2	1.16 ± 0.08	1.1 ± 0.1
Fe	828 ± 40	891 ± 30	900 ± 50	0.93 ± 0.05	0.92 ± 0.06
Ni	50 ± 1	46 ±1	44 ± 6	1.08 ± 0.03	1.1 ± 0.1
Cu	50 ± 1	53 ± 1	45 ± 6	0.94 ± 0.02	1.1 ± 0.1
Zn	50 ± 1	53 ± 1	45 ± 7	0.94 ± 0.02	1.1 ± 0.1
Sn	15 ± 2	15 ± 3	18 ±3	1.0 ±0.2	0.8± 0.2
Hf	16 ± 1	17 ± 1	ND	0.94 ± 0.08	–
W	7.2 ± 0.7	7.3 ± 0.7	7 ± 1	0.98 ± 0.13	1.02± 0.17
Pb	67 ± 1	101 ± 1	92 ± 6	0.66 ± 0.01	0.72 ± 0.05

The TXRF-determined concentrations of the elements present in one of the Zr-2.5%Nb samples (Sample-A) are tabulated in Table 2. The elemental concentrations were determined using predetermined relative sensitivity values as illustrated in Fig. S1. The obtained TXRF results were also compared with those obtained using the FP method. From the table it can be seen that both analytical approaches (FP and relative sensitivity based method) provide similar results for trace elements.

Under the TXRF excitation geometry, the incident beam penetrates only a few nanometres below the surface. Although the sample surfaces were thoroughly cleaned, it is critical to ensure that our compositional elemental data are representative of the bulk composition of the Zr-alloys and indeed do not represent surface impurities only. GIXRF intensity profiles produced by recording the characteristic XRF intensity versus incident angle in the range from zero up to a few degrees exhibit a distinct pattern, whether the probed element represents a surface impurity or is a homogeneously distributed element within the bulk of the sample. For this reason, GIXRF measurements were carried out on the Zr-2.5%Nb alloy sample (Sample-A); Fig. 5(*a*) represents the normalized GIXRF intensity profile acquired within the angular range 0–4.5° for all the elements detected in the sample. Fig. 5(*b*) shows the normalized GIXRF intensity profile within the same angular range but for trace elements only for better clarity. From both figures it can be observed that, for all the elements, there is a sharp rise of the fluorescence intensity around the critical angle for external total reflection on the alloy surface, followed by a rather constant intensity, as expected for elements homogeneously distributed in the bulk (Pagels *et al.*, 2010).

In order to further validate the TXRF results by means of a bulk analysis technique, the samples were analyzed using DC arc carrier distillation atomic emission spectrometry (AES). Hf could not be determined using the DC arc carrier distillation AES technique as Hf is refractory in nature. The

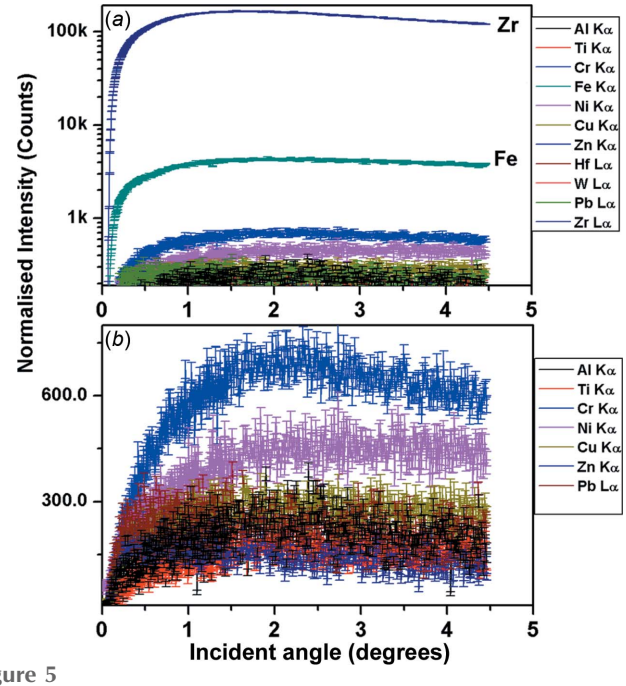

Figure 5
Normalized GIXRF intensity profile of the Zr-2.5% Nb sample in the angular range 0–4.5° for (*a*) all the elements and (*b*) trace elements only.

Table 3
Comparison of TXRF-determined concentrations using the relative sensitivity values and FP approaches with the DC arc carrier distillation method for different trace elements in Sample C: Zircalloy-4.

The values in '±' indicate a standard deviation of 1σ for n = 3 for TXRF measurements and 2σ for n = 3 for DC arc measurements.

	Concentrations				
Elements	RS (normal TXRF analysis) (A)	FP approach (B)	DC arc carrier distillation method (C)	A/B ratio	A/C ratio
Na	1.151 ± 0.002 (%)	1.04 ± 0.02 (%)	0.99 ± 0.09 (%)	1.10 ± 0.02	1.1 ± 0.1
Mg	410 ± 4 (p.p.m.)	360 ± 30 (p.p.m.)	450 ± 60 (p.p.m.)	1.1 ± 0.1	0.9 ± 0.1
Al	0.941 ± 0.008 (%)	0.854 ± 0.007 (%)	0.81 ± 0.07 (%)	1.10 ± 0.01	1.1 ± 0.1
Si	1.22 ± 0.03 (%)	1.23 ± 0.03 (%)	1.16 ± 0.09 (%)	0.99 ± 0.03	1.05 ± 0.08
Ti	124 ± 8 (p.p.m.)	113 ± 8 (p.p.m.)	120 ± 20 (p.p.m.)	1.1 ± 0.1	1.0 ± 0.2
Cr	0.28 ± 0.04 (%)	0.25 ± 0.04 (%)	0.22 ± 0.03 (%)	1.1 ± 0.2	1.2 ± 0.2
Mn	55 ± 6 (p.p.m.)	46 ± 5 (p.p.m.)	61 ± 8 (p.p.m.)	1.2 ± 0.2	0.9 ± 0.1
Fe	0.55 ± 0.01 (%)	0.59 ± 0.01 (%)	0.46 ± 0.07 (%)	0.93 ± 0.02	1.2 ± 0.2
Ni	159 ± 2 (p.p.m.)	147 ± 1 (p.p.m.)	140 ± 20 (p.p.m.)	1.08 ± 0.01	1.1± 0.1
Cu	488 ± 2 (p.p.m.)	498 ± 3 (p.p.m.)	500 ± 70 (p.p.m.)	0.97 ± 0.01	0.97 ± 0.13
Zn	0.37 ± 0.01 (%)	0.36 ± 0.01 (%)	0.36 ± 0.01 (%)	1.02 ± 0.04	1.02 ± 0.04
Sn	1.46 ± 0.03 (%)	1.47 ± 0.02 (%)	1.48 ± 0.02 (%)	0.99 ± 0.02	0.98 ± 0.02
W	36 ± 3 (p.p.m.)	37 ± 3 (p.p.m.)	37 ± 5 (p.p.m.)	0.9 ± 0.1	0.9 ± 0.1
Pb	519 ± 20 (p.p.m.)	781 ± 40 (p.p.m.)	700 ± 90 (p.p.m.)	0.66 ± 0.04	0.74 ± 0.09

trace, minor and major elemental concentrations of different elements present in the Zr-2.5%Nb (Sample-A) and Zircalloy-4 (Sample-C) alloy samples determined by the DC arc carrier distillation technique are also reported in Tables 2 and 3, expressed as a percentage (major) and in p.p.m. (trace and minor elements). It can be observed that the TXRF results of elemental concentrations deduced by means of relative sensitivities are in good agreement with those obtained using the FP approach and the DC arc carrier distillation AES technique. Moreover, it can also be noted from these tables that the TXRF analysis generally offers better precision in addition to its non-destructive nature for trace elemental concentrations below 100 p.p.m. compared with that of the DC arc carrier distillation AES.

The standard deviation (σ) of the ratio of two analytical values, *e.g.* A and B, shown in Tables 2 and 3 were calculated using the following formula,

$$\sigma = \left[\left(\frac{\sigma_1^2}{x_1^2} + \frac{\sigma_2^2}{x_2^2}\right)\right]^{1/2}, \qquad (2)$$

where σ_1 and σ_2 are the standard deviations of A and B, respectively, and x_1 and x_2 are the mean of A and B, respectively.

The analytical results of other Zr-2.5% Nb (Sample-B) and Zircalloy-4 (Sample-D) samples are tabulated in Table S1. It can again be observed that the relative sensitivity based TXRF analysis approach and the FP approach give similar results for almost all the elements in both the alloy samples.

The novel methodology reported in the present work is of great importance in terms of quality control of nuclear materials in a non-destructive manner with an added advantage of avoiding laborious dissolution of the samples. It can be extended to radioactive materials for minimizing the production of radio-analytical waste and radiation dose to the operator after proper modifications. In addition, the analysis shall be fast and economical as there are no costly materials required. The present study has been carried out using a synchrotron radiation source mainly for exploiting the advantages of available energy tunabilty. However, proper laboratory-based excitation sources can be chosen and optimized for similar work on a routine basis in the laboratory for quality control of such materials.

4. Conclusions

A novel, non-destructive TXRF methodology for the trace as well as major elemental determinations in Zircalloy-4 and Zr-2.5% Nb alloy samples has been developed. The approach avoids the time-consuming and laborious dissolution of samples and separation procedures. The developed methodology is very simple, fast, economical and straightforward. The elements ranging from Na (Z = 11) to Pb (Z = 82) present in the samples were quantified by applying the present, energy-selective TXRF-based analytical methodology, which improves the detection limits significantly compared with normal XRF determinations. It simplifies and improves the accuracy of such quantitative analysis by eliminating matrix corrections. It is imperative that the sample surface should be highly polished to attain proper experimental conditions.

In this work, we have reported the analytical results determined using predetermined relative sensitivity values as well as theoretically obtained values based on the fundamental parameter approach. The relative sensitivity and fundamental parameter-based approaches of concentration determinations gave similar analytical results. The methodology can be further extended for the trace as well as major elemental determinations of other different types of alloy materials like steel, inconel, *etc*., which have high technological importance. Although for this study we have used a synchrotron light source, not easily available for routine sample analysis, the method developed can be used for routine sample analysis in the laboratory with different suitable tube sources, detectors and vacuum sample chambers optimized for such applications.

Acknowledgements

The authors are thankful to Dr P. K. Pujari, Director, Radiochemistry and Isotope Group, and Dr S. Kannan, Head Fuel Chemistry Division, for their constant interest in this work. They gratefully acknowledge the International Atomic Energy Agency (IAEA) Coordination Research Project (CRP G42005) on the 'Experiments with synchrotron radiation

for modern environmental and industrial applications' for supporting the project through the research contract No. 18394, and the Elettra Sincrotrone, Trieste, Italy, for providing the access to the beamline through proposal No. 20145024. They are also thankful to the Department of Science and Technology (DST), Government of India, New Delhi, and International Centre for Theoretical Physics (ICTP), Trieste, Italy, for their financial support to visit Elettra for measurements. The authors would also like to acknowledge the XRF beamline staff for facilitating the delivery of optimum operational conditions for the synchrotron experiments and Dr Giuliana Aquilanti and Dr Ilaria Karlomagno for their kind discussions and assistance from time to time. The assistance of Dr R. Balasubramaniam (Control Systems Development Division, Bhabha Atomic Research Centre, Trombay, Mumbai 400085, India) for the measurements of surface roughness of polished Zircalloy samples is kindly acknowledged by the authors.

Funding information

The following funding is acknowledged: International Atomic Energy Agency; Department of Science and Technology (DST), Government of India, New Delhi; ICTP (International Centre for Theoretical Physics), Trieste, Italy.

References

Acharya, R., Nair, A., Reddy, A. & Goswami, A. (2004). *J. Nucl. Mater.* **326**, 80–85.
Al-Jobori, S. (1988). *J. Radioanal. Nucl. Chem.* **120**, 141–146.
Arsene, S., Bai, J. & Bompard, P. (2003). *Metall. Mater. Trans. A*, **34**, 553–566.
Banda, R., Lee, H. Y. & Lee, M. S. (2012). *Ind. Eng. Chem. Res.* **51**, 9652–9660.
Bertin, E. P. (2012). *Principles and Practice of X-ray Spectrometric Analysis.* Springer Science & Business Media.
Choudhuri, G., Srivastava, D., Gurumurthy, K. & Shah, B. (2008). *J. Nucl. Mater.* **383**, 178–182.
De Boer, D. K. G. & Van Den Hoogenhof, W. W. (1991). *Spectrochim. Acta B*, **46**, 1323–1331.
Dhara, S., Prabhat, P. & Misra, N. L. (2015). *Anal. Chem.* **87**, 10262–10267.
Ingerle, D., Meirer, F., Pepponi, G., Demenev, E., Giubertoni, D., Wobrauschek, P. & Streli, C. (2014). *Spectrochim. Acta B*, **99**, 121–128.
Ingerle, D., Schiebl, M., Streli, C. & Wobrauschek, P. (2014). *Rev. Sci. Instrum.* **85**, 083110.
Iofrida, M. J., Carricondo, J., Ararat, C., Iribarren, M. & Corvalán, C. (2015). *Tecnol. Metal. Mater. Miner.* **12**, 216–221.
Jaklevic, J. M., Giauque, R. D. & Thompson, A. C. (1988). *Anal. Chem.* **60**, 482–484.
Karydas, A. & Paradellis, T. (1999). *AIP Conf. Proc.* **475**, 460–463.
Karydas, A. G., Czyzycki, M., Leani, J. J., Migliori, A., Osan, J., Bogovac, M., Wrobel, P., Vakula, N., Padilla-Alvarez, R., Menk, R. H., Gol, M. G., Antonelli, M., Tiwari, M. K., Caliri, C., Vogel-Mikuš, K., Darby, I. & Kaiser, R. B. (2018). *J. Synchrotron Rad.* **25**, 189–203.
Klockenkämper, R. & Von Bohlen, A. (2015). *Total Reflection X-ray Fluorescence Analysis and Related Methods*, 2nd ed. John Wiley & Sons, Inc.
Kregsamer, P. (1991). *Spectrochim. Acta B*, **46**, 1332–1340.
Leani, J. J., Robledo, J. I. & Sánchez, H. J. (2019). *Spectrochim. Acta B*, **154**, 10–24.
Leenaers, A. J. G. & de Boer, D. K. G. (1995). *X-ray Spectrom.* **26**, 115–121.
Lenka, S. D. (2012). *Analytical characterization of technologically important materials using TXRF and EDXRF.* PhD thesis, p. 18. Homi Bhabha National Institute, Anushakti Nagar, Mumbai, India.
Manjusha, R., Reddy, M., Shekhar, R. & Jaikumar, S. (2013). *J. Anal. At. Spectrom.* **28**, 1932–1939.
Misra, N. L. (2011). *Pramana J Phys.* **76**, 201–212.
Northwood, D. O. (1985). *Mater. Des.* **6**, 58–70.
Pagels, M., Reinhardt, F., Pollakowski, B., Roczen, M., Becker, C., Lips, K., Rech, B., Kanngießer, B. & Beckhoff, B. (2010). *Nucl. Instrum. Methods Phys. Res. B*, **268**, 370–373.
Pahlke, S., Fabry, L., Kotz, L., Mantler, C. & Ehmann, T. (2001). *At. Spectrosc.* **56**, 2261–2274.
Pathak, N., Adya, V., Thulasidas, S., Sengupta, A., Seshagiri, T. & Godbole, S. (2014). *Spectrochim. Acta B*, **35**, 17–24.
Paul, H., Darrieulat, M., Vanderesse, N., Lityńska, L. & Miszczyk, M. (2010). *Arch. Met. Mater.* **55**, 1007–1019.
Pianetta, P., Baur, K., Singh, A., Brennan, S., Kerner, J., Werho, D. & Wang, J. (2000). *Thin Solid Films*, **373**, 222–226.
Robinson, K. & Hall, E. F. (1987). *JOM*, **39**, 14–16.
Sanyal, K., Chappa, S., Pathak, N., Pandey, A. K. & Misra, N. L. (2018). *Spectrochim. Acta B*, **150**, 18–25.
Sanyal, K., Dhara, S. & Misra, N. L. (2017). *X-ray Spectrom.* **46**, 442–447.
Sanyal, K., Dhara, S. & Misra, N. L. (2018). *Anal. Chem.* **90**, 11070–11077.
Sanyal, K., Kanrar, B., Misra, N. L., Czyzycki, M., Migliori, A. & Karydas, A. (2017). *X-ray Spectrom.* **46**, 164–170.
Sanyal, K. & Misra, N. L. (2019). *Spectrochim. Acta B*, **155**, 44–49.
Sengupta, A., Adya, V., Seshagiri, T., Thulasidas, S., Godbole, S. & Natarajan, V. (2014). *J. Res. Spectrosc.* **2014**, 757111.
Sengupta, A., Ippili, T., Jayabun, S., Singh, M. & Thulasidas, S. (2016). *J. Radioanal. Nucl. Chem.* **310**, 59–67.
Shenkay, L. & Fuchung, C. (1990). *Spectrochim. Acta B*, **45**, 527–535.
Solé, V., Papillon, E., Cotte, M., Walter, P. & Susini, J. (2007). *Spectrochim. Acta B*, **62**, 63–68.
Steffan, I. & Vujicic, G. (1994). *J. Anal. At. Spectrom.* **9**, 785–789.
Szalóki, I., Radócz, G. & Gerényi, A. (2019). *Spectrochim. Acta B*, **156**, 33–41.
Szaloki, I., Utaka, T., Tsuji, Y. & Taniguchi, K. (1999). *Adv. X-ray Anal.* **41**, 812–821.
Vander Wall, E. & Whitener, E. B. (1959). *Dissolution of Zirconium and Zircaloy-2 in Nitric–Hydrofluoric Acid Mixtures at Reflux Temperatures.* Report No. IDO-14497. Idaho Falls: Phillips Petroleum Co. Atomic Energy Division.
Vekemans, B., Janssens, K., Vincze, L., Adams, F. & Van Espen, P. (1994). *X-ray Spectrom.* **23**, 278–285.
Weidinger, H. G. (2007). *7th International Conference on WWER Fuel Performance, Modeling and Experimental Support*, 17–21 September 2007, Albena, Bulgaria.
Wobrauschek, P. (2007). *X-ray Spectrom.* **36**, 289–300.
Yilmazbayhan, A., Delaire, O., Motta, A. T., Birtcher, R., Maser, J. & Lai, B. (2003). *J. Nucl. Mater.* **321**, 221–232.
Zaimovskii, A. (1978). *At. Energy*, **45**, 1165–1168.